Consequences of NMDA receptor deficiency can be rescued in the adult brain

Catharine A. Mielnik[1], Mary A. Binko[2], Rehnuma Islam[2], Emily M. Johansson[3], Adam J. Funk[4], Yuxiao Chen[1], Marija Milenkovic[1], Wendy Horsfall[1], Ruth A. Ross[1], Laurent Groc[3], Ali Salahpour[1], Robert E. McCullumsmith[4], Evelyn K. Lambe[2], and Amy J. Ramsey[1,2]

[1] Department of Pharmacology & Toxicology, University of Toronto, ON, M5S 1A8, Canada

[2] Department of Physiology, University of Toronto, Toronto, ON, M5S 1A8, Canada

[3]Interdisciplinary Institute for NeuroScience (IINS) CNRS, Université Bordeaux Segalen, 33000 Bordeaux, France

[4]Department of Neurosciences, University of Toledo, Toledo, OH 43614 USA

Corresponding Author:
Amy Ramsey
1 King's College Circle
Room 4302 Medical Sciences Building
Toronto, ON M5S 1A8 Canada
(416) 978-2509
a.ramsey@utoronto.ca

Summary Paragraph

N-methyl-D-aspartate receptors (NMDARs) are required to shape activity-dependent connections in the developing and adult brain[1–6]. Impaired NMDAR signaling through genetic or environmental insults causes a constellation of neurodevelopmental disorders that manifest as intellectual disability, epilepsy, autism, or schizophrenia[7–9]. It is not clear whether the developmental impacts of NMDAR dysfunction can be overcome by interventions in adulthood. This question is paramount for neurodevelopmental disorders arising from mutations that occur in the *GRIN* genes, which encode NMDAR subunits[8–10], and the broader set of mutations that disrupt NMDAR function. We developed a mouse model where a congenital loss-of-function allele of *Grin1* is restored to wildtype by gene editing with Cre recombinase. Rescue of NMDARs in adult mice yields surprisingly robust improvements in cognitive behaviors, including those that are refractory to treatment with current medications. These results suggest that neurodevelopmental disorders arising from NMDAR deficiency can be effectively treated in adults.

One in 100 children are born with a neurodevelopmental disorder[11], including diagnoses of autism spectrum disorder and pervasive developmental delay, which have a combined prevalence of 1/143 children[12]. Until recently, most children with global developmental delay were not given a more specific diagnosis that could predict treatment or long-term prognosis. Whole exome sequencing has revolutionized diagnostic assessment and has identified hundreds of genes that can cause intellectual disability and developmental delay through transmitted and *de novo* variants[13].

Through whole-exome sequencing, a new syndrome called *GRIN* encephalopathy has been identified that is caused by mutations in one of the seven *GRIN* genes that encode subunits for NMDA-type glutamate receptors (NMDARs). Deleterious missense and nonsense variants in *GRIN1*, *GRIN2A-D*, and *GRIN3A-B* cause encephalopathies that are often first diagnosed as intellectual disability, global developmental delay, epilepsy, autism, and/or schizophrenia[14]. The variants are often *de novo* mutations that act as dominant negatives to reduce NMDAR function, although some variants lead to a gain-of function by altered channel gating properties[14]. Regardless of the nature of the mutation, patients with these deleterious variants have a similar syndrome of intellectual disability, and additional symptoms such as epilepsy, autism, cortical visual impairment, and movement disorders[14].

The identification of pathogenic variants in a *GRIN* gene allows for target-directed pharmacological treatments where approved drugs are available, but gene editing may ultimately be the most effective method to treat neurodevelopmental disorders. The most important question for the future application of this technology towards neurodevelopmental disorders is the timing of intervention. It has been assumed that intervention should occur as early in development as is medically feasible, that waiting risks irremediable damage, and that adults with these conditions are beyond the reach of medical treatment to improve cognitive function. However, these assumptions have not been stringently tested. Currently, there are many adults with these disorders that might also benefit from gene therapy, and it is unknown whether the developmental consequences of disease-causing variants can be reversed in adulthood.

The ability to reverse developmental insults is likely to depend on the nature of the insult. For example, while adult rescue of Rett Syndrome gene *Mecp2* in mice reversed several phenotypes[15], adult rescue of *Shank3* in mice showed a more selective improvement to social behaviours[16]. Thus, it is conceivable that developmental insults to the NMDAR system cannot be overcome with adult intervention, considering the central role of this receptor. Indeed, NMDARs are required for the proper connectivity of developing sensory circuits in the thalamus and cortex[17–19], for the establishment of both inhibitory[20] and excitatory[21] synapses, and for the patterning of neuron dendritic arborizations[22].

Since there is strong evidence that NMDARs participate in many aspects of neurodevelopment, we asked whether developmental consequences of NMDAR deficiency could be reversed in adult mice. Specifically, we asked whether adult intervention could improve cognitive behaviours mediated by the cortex, since intellectual disability is a core symptom of patients with *GRIN1* encephalopathy. *GRIN1* encodes the essential subunit GluN1 that is present in all NMDARs, and null mutations of *GRIN1* are lethal in humans[8] and in mice[17,23]. Considering the well-established role of these receptors in development and synapse refinement, it would be predicted that NMDAR deficiencies caused by *GRIN1* mutations, in particular, would be refractory to adult intervention.

To directly answer whether the developmental consequences of NMDAR deficiency could be rescued in adults, we generated mice with a reversible hypomorphic mutation in *Grin1*, the essential subunit of all NMDARs. Our previous studies with a similar mouse model have shown that a 90% knockdown of functional NMDARs is achieved through the targeted insertion of a neo cassette in an intron of the *Grin1* gene[24]. In the new model, we added *lox*P sites flanking the neo cassette to make inducible excision of the mutation possible, so that Cre recombinase could restore the locus to wildtype in a conditional manner (Fig 1A,B).

We intercrossed these mice with Rosa26-CreERT2 mice that ubiquitously express a tamoxifen-inducible Cre recombinase. We first identified the tamoxifen regimen that robustly induced Cre activity throughout the brain using a Cre reporter line (Rosa26-

dTomato: Extended Data Figure 1). We then administered tamoxifen to all genotypes of mice at postnatal day 70 (PD70) and measured biochemical and behavioural endpoints at PD98 (4-week recovery). Four genotypes of mice were studied: *Grin1*$^{+/+}$ (WT), *Grin1*$^{+/+}$:CreTg (WTCre), *Grin1*$^{flneo/flneo}$ (*Grin1*^{KD}), and *Grin1*$^{flneo/flneo}$:CreTg (*Grin1*^{RESCUE}). We determined that WT and WTCre mice had similar biochemical and behavioural phenotypes in all of the subsequent studies (Extended Data Figure 2), and thus experimental results for WT, *Grin1*^{KD} and *Grin1*^{RESCUE} mice were compared. Studies were performed with both male and female mice of equal number and powered to study the effect of sex.

We determined the extent of molecular recovery of *Grin1* mRNA and GluN1 protein by FISH and IHC (Figure 1C), and the levels of NMDAR by radioligand binding (Extended Data Figure 3). Importantly for our experimental objective, we observed substantial rescue of *Grin1* mRNA and NMDAR protein complex in the prefrontal cortex (PFC) of *Grin1*^{RESCUE} mice (Figure 1C and Extended Data Figure 3), providing the ability to test whether cortical functions could recover from developmental NMDAR deficiency.

The extent of NMDAR recovery in the cortex was further determined through whole cell electrophysiological recordings from brain slices. Physiological recordings from layer V pyramidal neurons of medial PFC (mPFC) were performed (Figure 2A). Bath applied NMDA elicited an inward current in wildtype cells. This current was greatly attenuated in *Grin1*^{KD} mice; however, in *Grin1*^{RESCUE} mice NMDA-elicited current was restored to wildtype levels (Figures 2B,C). The differences in functional NMDARs occurred in the presence of largely similar intrinsic membrane properties (Extended Data Table 1). However, capacitance was significantly larger in prefrontal neurons of *Grin1*^{RESCUE} compared to WT mice (Figure 2D). Accordingly, we analyzed the current density of the NMDA-elicited currents (Figure 2E; effect of genotype, $F_{2,95}$=3.6, p=0.03) and found that *Grin1*^{RESCUE} mice also had greatly increased current density compared to *Grin1*^{KD} mice.

As further demonstration of NMDAR recovery throughout the PFC, the levels of synaptic GluN1 were determined by immunoprecipitation with anti-PSD-95 antibody and mass spectrometry. This procedure isolates the proteins that are part of the PSD-95 post-synaptic protein complex, and specifically the amount of GluN1 peptide IVNIGAVLSTR

was determined relative to the intensity of PSD-95 peptides, to indicate the abundance of GluN1 protein at PFC synapses. As shown in Figure 2F, GluN1 peptide throughout the PFC was reduced in *Grin1*^{KD} mice and restored to wildtype levels in *Grin1*^{RESCUE} mice. Collectively, these results indicate that we achieved rescue of NMDAR deficiencies in the PFC and can test the ability of adult intervention to improve cognitive behaviours.

We studied several domains of cognition that are used as endophenotypes for autism and schizophrenia: habituation to a novel environment, sensory processing of acoustic startle, executive function, and social interaction. Although each of these behaviours relies on more than cortical function for their performance, previous studies have repeatedly demonstrated the critical role that the PFC plays in these cognitive tasks. Indeed, cell-selective knockout of NMDARs in cortical neurons is sufficient to impair habituation, sensory processing of acoustic startle, and social interaction[25–27].

Habituation to a novel environment requires the cortical and hippocampal processes of working and spatial memory to reduce exploration activity after a period of time[28,29]. Habituation was quantified by calculating the habituation index (H.I.), which is the time required to reach half of the maximal locomotor activity using linear regression. For *Grin1*^{KD} mice, the calculated H.I. was more than 120 minutes, because their hyperactivity persisted to the end of the test. *Grin1*^{KD} mice showed initial hyperactivity relative to WT in the first 10 minutes of exploration, and 120 minutes later, these mutant mice continued to explore the arena with high levels of activity (extrapolated H.I.: 149.1±15.6 min; Figure 3A). *Grin1*^{RESCUE} rescue mice also showed initial hyperactivity, but habituation was restored as indicated by a rate of habituation that was similar to WT mice (H.I.: WT 53.5±1.2 min, *Grin1*^{RESCUE} 64.4±3.2 min; Figure 3A, $p>0.99$, power=1.00).

Sensorimotor gating, which is modulated by cortical arousal circuits[30], was measured with the paradigm of pre-pulse inhibition (PPI) of acoustic startle response (ASR). Consistent with studies of the original knockdown mutation[31], *Grin1*^{KD} mice exhibited robust deficits in sensorimotor gating at pre-pulse intensities of 4, 8, and 16 dB (Figure 3B). This indicated that the pre-cognitive ability to attenuate motor response to a

startling sound was impaired. Importantly, *Grin1*^{RESCUE} mice showed a complete restoration of sensory processing in this test, with PPI levels that were similar to WT littermates (Figure 3B, p>0.99, power>0.99).

Executive function was tested in the puzzle box test, which measures the ability of the mouse to overcome increasingly challenging obstacles and reach a goal box. Mice were first introduced to the arena with an open doorway leading to the goal, but on subsequent tests the doorway was blocked, and mice had to use an underpass or dig through bedding to reach the goal. Thus, the test measured goal-directed behaviour and cognitive flexibility to respond to different challenges[32]. *Grin1*^{KD} mice routinely failed the most challenging task of digging through bedding and performed markedly worse than WT in all trials (Figure 3C). Impressively, *Grin1*^{RESCUE} mice solved both challenges, and performed significantly better than *Grin1*^{KD} mice on all trials (Figure 3C). Indeed, in three of the seven trials, *Grin1*^{RESCUE} mice performed similar to WT mice. Thus, there were substantial improvements in executive function as assessed in the puzzle box test. This provides evidence that the cognitive deficits resulting from the brain having developed without the normal complement of NMDARs are amenable to treatment.

Affiliative social behaviour was studied by measuring the amount of time that a mouse spent investigating a novel C57Bl/6J mouse. The novel mouse was constrained in one area with a wire cage, and an empty cage was included in the arena to control for non-social investigation of the cage. As expected, social interaction was significantly impaired in *Grin1*^{KD} mice relative to WT (Figure 3D). *Grin1*^{RESCUE} mice displayed social interaction that was completely restored to WT levels (p>0.99, power=1.00). Furthermore, *Grin1*^{KD} mutant mice showed excessive interest in exploring the arena and the empty cage as represented by the activity trace in Figure 3D, and the time spent per visit with the novel mouse was substantially reduced compared to WT (Figure 3D). Not only was the amount of time spent in social interaction normalized in *Grin1*^{RESCUE} mice, but the quality of social interaction appeared to improve, as demonstrated by the longer time spent with each visit to the novel mouse (Figure 3D).

We observed similar patterns of behavioural deficits in male and female *Grin1*^{KD} mice, and similar patterns of recovery in *Grin1*^{RESCUE} male and female mice in most tests.

There were notable sex differences in a select behavioural test, the puzzle box test, where female mice performed better than male mice irrespective of genotype (Extended Data Figure 4). It should also be noted that, in the puzzle box test, the female *Grin1*^{RESCUE} mice showed a greater improvement than male *Grin1*^{RESCUE} mice. Across both replications, however, there was significant and substantial improvement achieved in both sexes by the adult intervention.

Finally, we asked whether these behavioural improvements were replicable and robust. In a new cohort of experimental and control mice, as illustrated in the schematic in Extended Data Figure 5, we induced Cre-mediated rescue of *Grin1* at PD70 as in the original paradigm but waited an additional month before testing the animals (8-week recovery). In this cohort, there was a similar degree of rescue in the level of NMDARs (Extended Data Table 2). Behaviourally, the *Grin1*^{RESCUE} mice showed significant improvement across all measures examined (Extended Data Figure 5), in a pattern consistent with the assessment in Figure 3. This experiment shows that adult intervention can lead to replicable and robust cognitive improvement.

The knockdown of *Grin1* results in viable mutant mice with robust deficits in cognitive behaviours that parallel the symptoms of *GRIN1* encephalopathy[8]. Importantly, we did not find evidence of any deleterious effects from the postnatal upregulation of NMDARs. As would be expected from successful rescue, the *Grin1*^{RESCUE} mice appeared healthier and were less reactive to handling after Cre induction. We found improvements in every aspect of behaviour that we examined.

Our results provide striking evidence of the plasticity of the adult brain, particularly in the prefrontal cortex. It is possible that very early interventions would provide a more complete recovery of some brain functions. However, our current results suggest that symptoms of intellectual disability, a consistent symptom of *GRIN* encephalopathies[14], can be largely treated with adult intervention. This is surprising since cognitive impairments are refractory to current pharmacological treatment in patients with autism and schizophrenia[33], two conditions associated with impaired NMDAR function[34].

The prevalence of coding variants in *GRIN1,* or in the other *GRIN* genes, is unknown. The first patients to be sequenced had diagnoses of epilepsy and intellectual disability[8].

A recent whole-exome sequencing study reported that 7% of patients with autism or schizophrenia carry a predicted deleterious coding mutation in one of six GRIN genes (25/370 patients with schizophrenia, 15/192 patients with autism)[35]. There have also been numerous genetic and epidemiological studies supporting a causal role for NMDARs in several neuropsychiatric disorders. Thus, the significance of our findings is not limited to those patients who have been sequenced to date.

This study highlights the significant potential of therapeutic intervention in adult patients. It demonstrates that a delay between symptom onset and treatment can be overcome. The cognitive symptoms of neuropsychiatric and neurodevelopmental conditions caused by NMDAR hypofunction are amenable to treatment and show persisting improvement. The mature cortex has sufficient plasticity to recover from insults to this key developmental system, and adult intervention with the appropriate therapeutic agent should treat intellectual disabilities.

Acknowledgments

The authors would like to acknowledge Beverly Koller for donation of the pXena targeting construct, and Marc Caron, Bob Lefkowitz, Michael Didriksen, Jean-Martin Beaulieu, and Stephane Angers for helpful discussion. The authors would like to acknowledge Chinmaya Sadangi and Nirun Sivananthan for their preliminary work on RNAscope microscopy. This work was supported by CIHR funding to AJR (MOP119298), EKL (MOP89825 and CRC in Developing Cortical Physiology) and AS (MOP206649) and by NIMH to REM and AJF (MH107916 and L.I.F.E.). The work was also supported by graduate scholarships from CIHR and OGS to CAM, OMRI to MAB and a postdoctoral fellowship from Stiftelsen Olle Engkvist Byggmästare to EMJ.

REFERENCES

1. Tang, Y. P. *et al.* Genetic enhancement of learning and memory in mice. *Nature* **401,** 63–69 (1999).

2. Hubel, D. H. & Wiesel, T. N. Receptive Fields Of Cells In Striate Cortex Of Very Young, Visually Inexperienced Kittens. *J. Neurophysiol.* **26,** 994–1002 (1963).

3. Crair, M. C. & Malenka, R. C. A critical period for long-term potentiation at thalamocortical synapses. *Nature* **375,** 325–328 (1995).

4. Tsumoto, T., Hagihara, K., Sato, H. & Hata, Y. NMDA receptors in the visual cortex of young kittens are more effective than those of adult cats. *Nature* **327,** 513–514 (1987).

5. Cline, H. T., Debski, E. A. & Constantine-Paton, M. N-methyl-D-aspartate receptor antagonist desegregates eye-specific stripes. *Proc. Natl. Acad. Sci.* **84,** 4342–4345 (1987).

6. Goodman, C. S. & Shatz, C. J. Developmental mechanisms that generate precise patterns of neuronal connectivity. *Cell* **72,** 77–98 (1993).

7. Olney, J. W., Wozniak, D. F., Jevtovic-Todorovic, V. & Ikonomidou, C. Glutamate signaling and the fetal alcohol syndrome. *Mental Retardation and Developmental Disabilities Research Reviews* **7,** 267–275 (2001).

8. Lemke, J. R. *et al.* Delineating the GRIN1 phenotypic spectrum: A distinct genetic NMDA receptor encephalopathy. *Neurology* **86,** 2171–2178 (2016).

9. Lehesjoki, A.-E. *et al.* GRIN2B encephalopathy: novel findings on phenotype, variant clustering, functional consequences and treatment aspects. *J. Med. Genet.* **54,** 460–470 (2017).

10. Yuan, H., Low, C.-M., Moody, O. A., Jenkins, A. & Traynelis, S. F. Ionotropic GABA and Glutamate Receptor Mutations and Human Neurologic Diseases. *Mol. Pharmacol.* **88,** 203–217 (2015).

11. Maulik, P. K., Mascarenhas, M. N., Mathers, C. D., Dua, T. & Saxena, S. Prevalence of intellectual disability: A meta-analysis of population-based studies. *Research in Developmental Disabilities* **32,** 419–436 (2011).

12. Fombonne, E. Epidemiology of pervasive developmental disorders. *Pediatric Research* **65,** 591–598 (2009).

13. Mohammed, S. *et al.* Large-scale discovery of novel genetic causes of developmental disorders. *Nature* **519,** 223–228 (2014).

14. XiangWei, W., Jiang, Y. & Yuan, H. De novo mutations and rare variants occurring in NMDA receptors. *Current Opinion in Physiology* **2,** 27–35 (2018).

15. Guy, J., Gan, J., Selfridge, J., Cobb, S. & Bird, A. Reversal of neurological defects in a mouse model of Rett syndrome. *Science (80-.).* **315,** 1143–1147 (2007).

16. Mei, Y. *et al.* Adult restoration of Shank3 expression rescues selective autistic-like phenotypes. *Nature* **530,** 481–484 (2016).

17. Li, Y., Erzurumlu, R. S., Chen, C., Jhaveri, S. & Tonegawa, S. Whisker-related neuronal patterns fail to develop in the trigeminal brainstem nuclei of NMDAR1 knockout mice. *Cell* **76,** 427–437 (1994).

18. Suzuki, A. *et al.* Thalamic NMDA Receptor Function Is Necessary for Patterning of the Thalamocortical Somatosensory Map and for Sensorimotor Behaviors. *J. Neurosci.* **34,** 12001–12014 (2014).

19. Iwasato, T. *et al.* Cortex-restricted disruption of NMDAR1 impairs neuronal patterns in the barrel cortex. *Nature* **406,** 726–731 (2000).

20. Gu, X., Zhou, L. & Lu, W. An NMDA Receptor-Dependent Mechanism Underlies Inhibitory Synapse Development. *Cell Rep.* **14,** 471–478 (2016).

21. Zhang, Z. -w., Peterson, M. & Liu, H. Essential role of postsynaptic NMDA receptors in developmental refinement of excitatory synapses. *Proc. Natl. Acad. Sci.* **110,** 1095–1100 (2013).

22. Espinosa, J. S., Wheeler, D. G., Tsien, R. W. & Luo, L. Uncoupling Dendrite Growth and Patterning: Single-Cell Knockout Analysis of NMDA Receptor 2B. *Neuron* **62,** 205–217 (2009).

23. Forrest, D. *et al.* Targeted disruption of NMDA receptor 1 gene abolishes NMDA response and results in neonatal death. *Neuron* **13,** 325–338 (1994).

24. Mohn, A. R., Gainetdinov, R. R., Caron, M. G. & Koller, B. H. Mice with reduced NMDA receptor expression display behaviors related to schizophrenia. *Cell* **98,** 427–436 (1999).

25. Rompala, G. R., Zsiros, V., Zhang, S., Kolata, S. M. & Nakazawa, K. Contribution of NMDA Receptor Hypofunction in Prefrontal and Cortical Excitatory Neurons to Schizophrenia-Like Phenotypes. *PLoS One* **8,** e61278 (2013).

26. Belforte, J. E. *et al.* Postnatal NMDA receptor ablation in corticolimbic interneurons confers schizophrenia-like phenotypes. *Nat. Neurosci.* **13,** 76–83 (2010).

27. Finlay, J. M. *et al.* Effects of prefrontal cortex and hippocampal NMDA NR1-subunit deletion on complex cognitive and social behaviors. *Brain Res.* **1600,** 70–83 (2015).

28. Yamaguchi, S., Hale, L. A., D'Esposito, M. & Knight, R. T. Rapid prefrontal-hippocampal habituation to novel events. *J. Neurosci.* **24,** 5356–63 (2004).

29. Ranganath, C. & Rainer, G. Cognitive neuroscience: Neural mechanisms for detecting and remembering novel events. *Nat. Rev. Neurosci.* **4,** 193–202 (2003).

30. Li, L., Du, Y., Li, N., Wu, X. & Wu, Y. Top-down modulation of prepulse inhibition of the startle reflex in humans and rats. *Neuroscience and Biobehavioral Reviews* **33,** 1157–1167 (2009).

31. Duncan, G. E. *et al.* Deficits in sensorimotor gating and tests of social behavior in a genetic model of reduced NMDA receptor function. *Behav. Brain Res.* **153,** 507–519 (2004).

32. Ben Abdallah, N. M.-B. *et al.* The puzzle box as a simple and efficient behavioral test for exploring impairments of general cognition and executive functions in mouse models of schizophrenia. *Exp. Neurol.* **227,** 42–52 (2011).

33. Millan, M. J. *et al.* Cognitive dysfunction in psychiatric disorders: characteristics, causes and the quest for improved therapy. *Nat. Rev. Drug Discov.* **11,** 141–68 (2012).

34. Tarabeux, J. *et al.* Rare mutations in N-methyl-D-aspartate glutamate receptors in autism spectrum disorders and schizophrenia. *Transl. Psychiatry* **1,** e55 (2011).

35. Yu, Y. *et al.* Rare loss of function mutations in N-methyl-d-aspartate glutamate receptors and their contributions to schizophrenia susceptibility. *Transl. Psychiatry* **8,** 12 (2018).

36. Franklin, K. B. J. & Paxinos, G. *Paxinos and Franklin's The mouse brain in stereotaxic coordinates*.

37. Ventura, A. *et al.* Restoration of p53 function leads to tumour regression in vivo. *Nature* **445,** 661–665 (2007).

38. Madisen, L. *et al.* A robust and high-throughput Cre reporting and characterization system for the whole mouse brain. *Nat. Neurosci.* **13,** 133–140 (2010).

39. Silva, A. J. *et al.* Mutant mice and neuroscience: Recommendations concerning genetic background. *Neuron* **19,** 755–759 (1997).

40. Islam, R. *et al.* Vulnerability to omega-3 deprivation in a mouse model of NMDA

receptor. *npj Schizophr.* **3,** 12 (2017).

41. Milenkovic, M., Mielnik, C. A. & Ramsey, A. J. NMDA receptor-deficient mice display sexual dimorphism in the onset and severity of behavioural abnormalities. *Genes, Brain Behav.* **13,** 850–862 (2014).

42. Mielnik, C. A., Horsfall, W. & Ramsey, A. J. Diazepam improves aspects of social behaviour and neuron activation in NMDA receptor-deficient mice. *Genes, Brain Behav.* **13,** 592–602 (2014).

43. DeBlasi, A., O'Reilly, K. & Motulsky, H. J. Calculating receptor number from binding experiments using same compound as radioligand and competitor. *Trends Pharmacol. Sci.* **10,** 227–229 (1989).

44. Sullivan, C. R. *et al.* Connectivity Analyses of Bioenergetic Changes in Schizophrenia: Identification of Novel Treatments. *Molecular Neurobiology* (2018). doi:10.1007/s12035-018-1390-4

MATERIALS AND METHODS

Generation of *Grin1* Inducible-Rescue Mice (*Grin1*$^{flneo/flneo}$)

Animal housing and experimentation were carried out in accordance with the Canadian Council in Animal Care (CCAC) guidelines for the care and use of animals and following protocols approved by the Faculty of Medicine and Pharmacy Animal Care Committee at the University of Toronto. Mice were group housed with littermates on a 12-h light-dark cycle (0700 to 1900h) and were given *ad libitum* access to food (2018 Teklad Global 18% Protein Rodent Diet, Envigo, Madison Wisconsin USA, www.envigo.com). Tail biopsy for genotyping and toe tattooing for identification was performed at PD13 (± 3 days) and mice were weaned at P21.

ROSA26^{CreERT2} mice were obtained from Jackson Laboratory (008463; B6.129-*Gt(ROSA)26Sor*$^{tm1(cre/ERT2)Tyj}$*/J*), and were previously described[37]. Mice harboring the Cre transgene were identified by PCR of genomic DNA using the following primers: common forward 5'- AAA GTC GCT CTG AGT TGT TAT-3', wildtype reverse 5'- GGA GCG GGA GAA ATG GAT ATG-3', mutant reverse 5'- CCT GAT CCT GGC AAT TTC G-3'.

The Cre-reporter mouse line used, *ROSA26*^{tdTomato}, was obtained from Jackson Laboratory (007914; B6.Cg-*Gt(ROSA)26Sor*$^{tm14(CAG-tdTomato)Hze}$/J) and was crossed with the *ROSA26*^{CreERT2} line. The mouse line expresses tdTomato following Cre-mediated recombination. This mouse line was used to ensure ubiquitous activation of Cre following tamoxifen administration as previously described[38]. Mice harboring the Cre-reporter transgene were identified by PCR of genomic DNA using the following primers: wildtype forward 5'- AAG GGA GCT GCA GTG GAG TA-3', wildtype reverse 5'- CCG AAA ATC TGT GGG AAG TC-3', mutant forward 5'- GGC ATT AAA GCA GCG TAT CC-3', mutant reverse 5'- CTG TTC CTG TAC GGC ATG G-3'.

Grin1$^{flneo/flneo}$ mice were generated at the University of Toronto, based on the previously described *Grin1*$^{neo/neo}$ mouse[24]. Identical to the *Grin1*$^{neo/neo}$ model, the *Grin1* gene was modified via homologous recombination with an intervening sequence (neomycin cassette), and targeted into intron 19, but this time flanked by *loxP* sites, so the insertion mutation could be excised following Cre-recombination. The vector (pXena; gift of Dr. Beverly Koller) contained a floxed neomycin resistance gene. Homologous arms of intron 19 of the *Grin1* gene were PCR-amplified from mouse genomic DNA and cloned into the vector flanking the floxed neomycin cassette. The linearized targeting construct was electroporated into mouse ES cells (129/SvlmJ

strain) by The Centre for Phenogenomics (TCP, Toronto, ON). G418 was used for positive selection of targeted ES cells. Drug resistant clones were screened by PCR, and homologous recombination was confirmed by Southern blot analysis (data not shown). Correctly targeted ES cell clones were used to make chimeras by diploid aggregation (TCP), which were subsequently bred to 129/SvlmJ female mice to obtain ES cell germline-transmitted offspring, determined by PCR genotyping. The floxed insertion mutation (neo) was identified using the following primers: wildtype forward 5'- TGA GGG GAA GCT CTT CCT GT-3', mutant forward 5'- GCT TCC TCG TGC TTT ACG GTA T-3', common reverse 5'-AAG CGA TTA GAC AAC TAA GGG T-3'.

Germline transmitting chimeras were crossed directly with 129/SvlmJ mice to produce *Grin1*$^{+/flneo}$ 129/SvlmJ congenics. Mice were also crossed to C57Bl/6J wildtypes for at least 6 generations to produce C57Bl/6J *Grin1*$^{+/flneo}$ congenics. Subsequently, *Grin1*$^{+/flneo}$: CreTg mice were produced by crossing *ROSA26*^{CreERT2} C57Bl/6J congenic mice to *Grin1*$^{+/flneo}$ C57Bl/6J congenics. The resulting compound heterozygotes were bred to *Grin1*$^{+/flneo}$ 129/SvlmJ congenics to produce the F1 progeny used for all experiments. Use of an F1 genetic background is recommended by the Banbury Conference[39] and is experimentally required since there is a high mortality rate for homozygous mutant *Grin1* mice on the C57Bl/6J background.

Tamoxifen Administration

Tamoxifen was administered to all genotypes of mice (WT, WTCre, *Grin1*^{KD}, *Grin1*^{RESCUE}). Tamoxifen (T5648, Sigma-Aldrich, St. Louis, MO, USA) was administered via oral gavage (6mg, 20mg/ml dissolved in 100% corn oil at 65°C for 1 hour) on day 1 of treatment, and then mice were given tamoxifen chow (TD.140425, 500mg/kg, Envigo) *ad libitum* for 14 days. Following tamoxifen administration, mouse toenails were trimmed every two weeks to prevent the skin lesions that otherwise occur due to excessive grooming of *Grin1*^{KD} and *Grin1*^{RESCUE} mice.

Behavioural Testing

Male and female mice of equal numbers were used for behavioural testing. Tests were administered at PD98 or PD126, as specified. Behavioural tests were conducted between 09:00 and 15:00h. All experimental animals were first tested for locomotor activity on Day 1 of behavioural assessment. Mice were then assigned to one of two groups for subsequent behavioural tests that spanned three days. The puzzle box test was administered to mice in Group A over Days 2-4. Mice in Group B were tested in the elevated plus maze (data not

shown) on Day 2, the social affiliative paradigm on Day 3, and pre-pulse inhibition of acoustic startle on Day 4.

Open Field Test: Locomotor activity was measured as previously described[40,41], using digital activity monitors (Omnitech Electronics, Columbus, OH, USA) on the first day of testing. Naïve mice were placed in novel Plexiglas arenas (20 x 20 x 45 cm) and their locomotor and stereotypic activity were recorded over a 120-min period in dim light (15-16 lux). Activity was tracked via infrared light beam sensors; total distance travelled and stereotypic movements were collected in 5-minute bins. The habituation index was calculated by the time to ½ of maximal activity by linear regression using GraphPad Prism.

Puzzle Box Assay: The puzzlebox test was used to assess executive function[32] as previously described[40,41]. The puzzle box arena contained a brightly lit area (250 lux, 58 x 28 x 27.5 cm), and a dimly lit area termed the goal box (5 lux, 14 x 28 x 27.5 cm). The two areas were separated by a black Plexiglas divider, and increasingly difficult barriers were presented to the mice. Mice were placed in the lighted area and the time required for the mouse to reach the goal box was scored manually with a 300 second cut-off. The first trial measured the time required to reach the goal when a doorway gave access to the goal box. The second, third, and fourth trials measured the time required to reach the goal when the only access to the goal box was an underpass. The fifth, sixth, and seventh trials measured the time required to reach the goal box when the underpass was blocked with bedding. The inter-trial interval for trials 2, 3, 5 and 6 was two minutes. The inter-trial interval for trials 4 and 7 was 24 hours.
Thus the trials for the puzzle box were as follows;
Day 1: T1 open door and underpass, T2 and T3 underpass only access.
Day 2: T4 underpass only, T5 and T6 underpass filled with bedding.
Day 3: T7 underpass filled with bedding.

Affiliative Social Interaction: Affiliative social behaviour was assessed as previously described[40–42]. Sociability was measured with videotracking software Biobserve Viewer2, with the body center used as the reference point. Experimental mice were allowed to explore the open area (opaque white walls, 62 x 42 x 22 cm) for 10-min in dim lighting (15-16 lux). The area contained two inverted wire cups, one containing a stimulus mouse (‘social’) and the other empty (‘non-social’). Time spent in each zone (3 cm zone around the cup) was recorded with the Biobserve

software. The mice that were used as a social stimulus were novel, wildtype, C57Bl/6 mice that were age- and sex-matched to the test mouse.

Pre-Pulse Inhibition/Startle Reflex: Pre-pulse inhibition of the acoustic startle response was measured with SR-LAB equipment and software from San Diego Instruments, as previously described[40]. Briefly, accelerometers were calibrated to 700±5 mV and output voltages were amplified and analyzed for voltage changes using SR Analysis (San Diego Instruments, San Diego, CA, USA). Background white noise was maintained at 65dB. PPI was measured in a 30-min test with 80 randomized trials of: (1) 10 trials pulse alone (2) 10 trials pre-pulse alone (for each pre-pulse), (3) 10 trials pre-pulse plus pulse (for each pre-pulse), and (4) 10 trials no pulse. 5 pulse alone trials were performed before and after the 80 trials, totaling 90 trials per run. The pre-pulse (4dB, 8dB, or 16dB above 65dB background) was presented 100ms prior to the startle pulse (100dB above 65dB background). The inter-stimulus interval (ISI) was randomized between 5 and 20s. Experimental mice were placed in a cylindrical tube on a platform in a soundproof chamber. Mice were allowed to acclimatize in the chamber and to the background noise for 300s, followed by 5 consecutive pulse alone trials, then by 80 randomized trials (as described above) and then 5 consecutive pulse alone trials. Pre-pulse inhibition was measured as a decrease in the amplitude of startle response to a 100dB acoustic startle pulse, following each pre-pulse (4dB, 8dB and 16dB).

Harvesting Whole Brain Tissue

Mice were euthanized by cervical dislocation on the day subsequent to the last behavioural test. Brains were removed and frozen in dry-ice chilled 2-methylbutane (Sigma Aldrich). Brains were stored in 5ml eppendorf tubes at -80°C before use in: radioligand binding, immunohistochemistry, western blot, *in situ* hybridization, and PSD-95 pull-down experiments.

Immunoflourescent detection of Cre recombinase activity

Mice carrying the *ROSA26*^{tdTomato} and *ROSA26*^{CreERT2} alleles were generated and administered tamoxifen as described above. Three days after tamoxifen treatment, animals were euthanized by perfusion fixation under anesthesia. Mice were anaesthetized with 250mg/kg Avertin, which was composed of [2,2,2-tribromoethanol (Sigma Aldrich) dissolved in 2-methyl-2-butanol (Sigma Aldrich) 2.5% v/v)]. Whole brains were perfused with 4% paraformaldehyde (PFA), post-fixed in PFA for 3 hours at 4°C and then transferred to 30% sucrose for three days at 4°C. Frozen sections of 40µm were collected (coronal sections at Bregma 1.78mm, 1.10mm, -1.94mm, -

6.00mm). Sections were mounted and visualized using Nikon Elements software (NIS-Elements Basic Research, version 3.1).

RNAscope Visualization of *Grin1* mRNA

Expression of *Grin1* mRNA in WT, *Grin1*^{KD}, and *Grin1*^{RESCUE} mice was visualized by fluorescent in situ hybridization largely following the RNAscope Multiplex Fluorescent Reagent Kit v2 protocol (ACD Bio; CA, USA). Frozen mouse brains (as described above) were processed with a cryostat to produce 20µm saggital sections at 1.2 mm from midline that were mounted onto SuperFrost Plus charged slides (Fisher Scientific). Sections were fixed by submersion in 4% paraformaldehyde, dehydrated in ethanol, incubated in 0.3% hydrogen peroxide, and treated with RNAscope Protease IV. Sections were hybridized to *Grin1* probes (product reference ID 533691, ACD Bio) or to control probe mixtures (positive control probes reference ID 320881, negative control probes reference ID 320871). Signal was detected with TSA Plus cyanine 3 (PerkinElmer, Llantrisant, UK) and horseradish peroxidase. Vectashield with DAPI mounting medium was used (Vector Laboratories, CA, USA). Processed slides were stored at 4˚C overnight before imaging at 20X magnification with an Axio Scan.Z1 slide scanner (Zeiss, Oberkochen, DEU).

Immunofluorescent Visualization of GluN1 Protein

Expression of GluN1 protein levels in WT, *Grin1*^{KD} and *Grin1*^{RESCUE} mice were visualized by fluorescent immunohistochemistry. Sagittal tissue sections (20µm thick; Lateral ~1.92mm) were cut on a microtome-cryostat, thaw-mounted onto SuperFrost Ultra Plus adhesion slides (Thermo Scientific, MA, USA), and stored at -20°C until further processing. In brief, after fixation at 4°C in 4% paraformaldehyde, the sections were subjected to a heat-induced epitope retrieval protocol by submerging the slides in Tris-EDTA-SDS buffer (10mM TrisBase, 1mM EDTA, 0.05% SDS, pH 9.0) for 7-min at 96°C. After slowly reducing the temperature, blocking was carried out for 1-hour in Tris-Buffered Saline (TBS) solution in 0.3M glycine containing 10% normal goat serum (Sigma-Aldrich, #G3023, Lot:SLBR1636V, MI, USA). Incubation with a rabbit anti-GluN1 antibody (in-house antibody, 1:200) was done in a TBS solution containing 10% normal goat serum overnight at 4°C. Staining with secondary antibody, anti-rabbit Alexa 568 (ThermoFisher, #A11011, Lot:1670154, 1:500), was performed for 1-hour at room temperature, and slides were mounted with DAPI-containing Vectashield. Image acquisition was done on a video spinning-disk system (Leica DMI6000B, 40X). Figures were assembled in ImageJ (NIH) and a fixed threshold was applied for generation of images from different conditions. Adobe Photoshop

(Adobe Systems, CA, USA) was used for composition, only contrast and brightness were adjusted to optimize the image quality.

[^{3}H]MK-801 Saturation Binding Assay

Prefrontal cortex and hippocampus were dissected from frozen brains (see previous section). Each brain region was pooled from two separate animals (cortex from two separate mice were pooled for a single n within each genotype). Tissue was homogenized in binding buffer (20mM HEPES pH 7.4, 1mM EDTA pH 8.0, 0.1mM glycine, 0.1mM glutamate, 0.1mM spermidine, Aprotinin (1000x), Leupeptin (1000x), Pepstatin A (500x), Benzamidine (1000x) and PMSF (2500x)) using a standing homogenizer and glass Teflon homogenizer tubes followed by Polytron (PT-1200-E). Homogenate was centrifuged at 600 *g* for 10 min at 4°C. Supernatant was then centrifuged at 40000 *g* 15 min at 4°C. Pellet was washed with binding buffer and centrifuged at 40000 *g* for 15 min at 4°C. Pellets were resuspended in binding buffer without protease inhibitors and protein concentration was measured using BCA assay (Thermo Scientific). Membranes were diluted to a 1.6µg/µl working concentration and stored at -80°C.

For the [^{3}H]MK-801 saturation protein binding assay, working solutions of [^{3}H]MK-801 and cold MK-801 were prepared. [^{3}H]MK-801 (Perkin Elmer) was diluted to a working concentration of 120nM (final concentration 40nM) in binding buffer. Cold MK-801 (Sigma Aldrich) was prepared to a 1200nM working solution (final concentration 400nM; 10x [^{3}H]MK-801) in binding buffer. 80µg membranes were incubated with MK-801 and [^{3}H]MK-801 in binding buffer at 32°C for 3 hours before termination by the addition of ice-cold wash buffer (20mM HEPES pH 7.4, 1mM EDTA pH 8.0) and vacuum filtration using a 24-well sampling manifold (Brandel Cell Harvester) and Whatman GF/B glass-fibre filters (Brandel, MD, USA) soaked in 0.05% polyethylenimine. Filters were placed in 5mL scintillation fluid (Ultima Gold XR, Perkin Elmer) and allowed to incubate overnight. Radioactivity was quantified via liquid scintillation spectrometry[43].

Postsynaptic GluN1 Peptide Levels

As previously described[44], a mouse anti-PSD-95 antibody (Millipore, catalogue # MAB1596) was used to capture PSD-95 protein complexes from samples (3 male and 3 female WT, 3 male and 3 female *Grin1*^{KD}, and 3 male and 3 female *Grin1*^{RESCUE}). The specificity of this antibody was verified using multiple reaction monitoring mass spectrometry analysis of PSD-95 peptides captured by affinity purification. 5 µg of PSD-95 antibody was coupled to 1 mg of Dynabeads (Life Technologies, CA, USA) according to the antibody coupling kit protocol (#14311D). For

each sample, 1000µl of 10mg/ml antibody coupled beads were washed 2x 1ml with ice cold 1x PBST (#9809S, Cell Signaling, MA, USA), then incubated with mouse brain lysate brought to a final volume of 1000µl with ice cold 1x PBST for 1 hour at room temperature. The supernatant was removed and the beads were washed 4 x 10 min at room temperature in 1ml ice cold 1x PBST. Captured protein complexes were eluted with 30µl of 1N Ammonium Hydroxide (#320145, Sigma-Aldrich), 5mM EDTA, pH 12 for 10 min at room temperature. 6µl of 6x protein denaturing buffer (4.5% SDS, 15% β-mercaptoethanol, 0.018% bromophenol blue, and 36% glycerol in 170 mM Tris-HCl, pH 6.8) was added to each sample elution. The eluted samples were heated at 70°C for 10-min then processed for mass spectrometry.

All samples were loaded on a 1.5 mm, 4-12% Bis-Tris Invitrogen NuPage gel (NP0335BOX) and electrophoresed in 1x MES buffer (NP0002) for 10-min at 180v. The gel was fixed in 50% ethanol/10% acetic acid overnight at RT, then washed in 30% ethanol for 10-min followed by two 10-min washes in MilliQ water (MilliQ Gradient system, Millipore, MA, USA). The lanes were harvested, cut into small (~2mm) squares, and subjected to in-gel tryptic digestion and peptide recovery. Samples were resuspended in 0.1% formic acid.

Nano liquid chromatography coupled electrospray tandem mass spectrometry (nLC-ESI-MS/MS) analyses were performed on a 5600+ QTOF mass spectrometer (Sciex, Toronto, ON, Canada) interfaced to an Eksigent (Dublin, CA, USA) nanoLC.ultra nanoflow system. Peptides were loaded (via an Eksigent nanoLC.as-2 autosampler) onto an IntegraFrit Trap Column (outer diameter of 360µm, inner diameter of 100µm, and 25 µm packed bed) from New Objective, Inc. (Woburn, MA, USA) at 2 µl/min in formic acid/H_2O 0.1/99.9 (v/v) for 15-min, to desalt and concentrate the samples. For the chromatographic separation of peptides, the trap-column was switched to align with the analytical column, Acclaim PepMap100 (inner diameter of 75µm, length of 15cm, C18 particle sizes of 3µm and pore sizes of 100Å) from Dionex-Thermo Fisher Scientific (Sunnyvale, CA, USA). The peptides were eluted using a variable mobile phase (MP) gradient from 95% phase A (Formic acid/H_2O 0.1/99.9, v/v) to 40% phase B (Formic Acid/Acetonitrile 0.1/99.9, v/v) for 70-min, from 40% phase B to 85% phase B for 5-min, and then keeping the same mobile phase composition for 5 additional minutes at 300 nL/min. The nLC effluent was ionized and sprayed into the mass spectrometer using NANOSpray® III Source (Sciex). Ion source gas 1 (GS1), ion source gas 2 (GS2) and curtain gas (CUR) were respectively kept at 8, 0 and 35 vendor specified arbitrary units. The mass spectrometer method was operated in positive ion mode and the interface heater temperature and ion spray voltage

were kept at 150ºC, and at 2.6kV, respectively. The data was recorded using Analyst-TF (version 1.7) software.

The data independent acquisition (DIA) method was set to go through 1757 cycles for 99-min, where each cycle performed one TOF-MS scan type (0.25 second accumulation time, in a 550.0 to 830.0 m/z window) followed by 56 sequential overlapping windows of 6 Daltons each. Note that the Analyst software automatically adds 1 Dalton to each window to provide overlap, thus an input of 5 Da in the method set up window results in an overlapping 6 Da collection window width (e.g. 550-556, then 555-561, 560-566, etc). Within each window, a charge state of +2, high sensitivity mode, and rolling collision energy with a collision energy spread (CES) of 15 V was selected. The resulting data were analyzed by Sciex DIA software to generate peptide intensities.

Electrophysiological Recordings

Mice (WT, *Grin1*^{KD}, and *Grin1*^{RESCUE} at PD70) were administered chloral hydrate (400 mg/kg) and euthanized by decapitation. The brain was removed from the skull and cooled in oxygenated sucrose-substituted ACSF. The brain was blocked to obtain the anterior portion and coronal slices (400 µm) of the medial prefrontal cortex (1.98 mm-1.34 mm)[36] were sectioned by the Dosaka Pro-7 Linear Slicer (SciMedia, CA, USA). The slices recovered for at least 1.5-hours in a chamber containing oxygenated ACSF (in mM: 128 NaCl, 10 D-glucose, 26 $NaHCO_3$, 2 $CaCl_2$, 1.25 NaH_2PO_4, 2 $MgSO_4$, 3 KCl) at 30°C before being transferred to the stage of an upright microscope for whole cell patch clamp recordings. Layer V pyramidal neurons in the medial prefrontal cortex were identified by infrared differential inference contrast microscopy. The whole cell patch pipettes (2-4 MΩ) contained the following intracellular solution (in mM): 120 potassium gluconate, 5 KCl, 2 MgCl, 4 K_2-ATP, 0.4 Na_2-GTP, 10 Na_2-phosphocreatine, and 10 HEPES buffer, adjusted to pH 7.33 with KOH.

For these experiments, the brain slices were continuously perfused with 30°C modified ACSF (in mM: 128 NaCl, 10 D-glucose, 26 $NaHCO_3$, 2 $CaCl_2$, 1.25 NaH_2PO_4, 0.5 $MgSO_4$, 5 KCl) to relieve the magnesium blockade in order to study NMDARs. Experiments were performed in the presence of CNQX disodium salt (20 µm; Alomone Labs, Israel) to block AMPA receptors. NMDA (30 µm; Sigma-Aldrich) was bath applied to assess NMDAR function. Application of APV (50 µM; Alomone Labs) confirmed the inward currents were mediated by NMDARs. The peak amplitude of the NMDA currents was measured using Clampfit software (Molecular Devices,

CA, USA). The magnitude of NMDA-elicited inward currents was quantified by subtracting a 1 second average holding current at the peak from the average holding current at the baseline.

Quantification and Statistical Analysis

Statistical parameters, the definition of measures and statistical significance are reported in the figures and the figure legends. Data are represented as mean ± SEM, as indicated in figure legends. Sample number (*n*), indicating independent biological samples (balanced for sex), are indicated in each figure and/or figure legend. Statistically significant outliers were calculated and excluded, using the Grubb's Test. Data were analyzed either using a one- or two-way ANOVA (repeated measures) where indicated, with multiple comparisons and post-hoc Bonferroni's test, as indicated in figure legends. For electrophysiological recordings, paired t-tests were used to compare neuronal responses to NMDA before and after APV. Data analysis was not blinded. Differences in means were considered statistically significant at $p<0.05$. Significance levels are as follows; *$p<0.05$, **$p<0.01$, ***$p<0.001$, ****$p<0.0001$, ns – not significant. All data analyses were performed using the Graphpad Prism 6.0 software and/or IBM SPSS 23.0 Software.

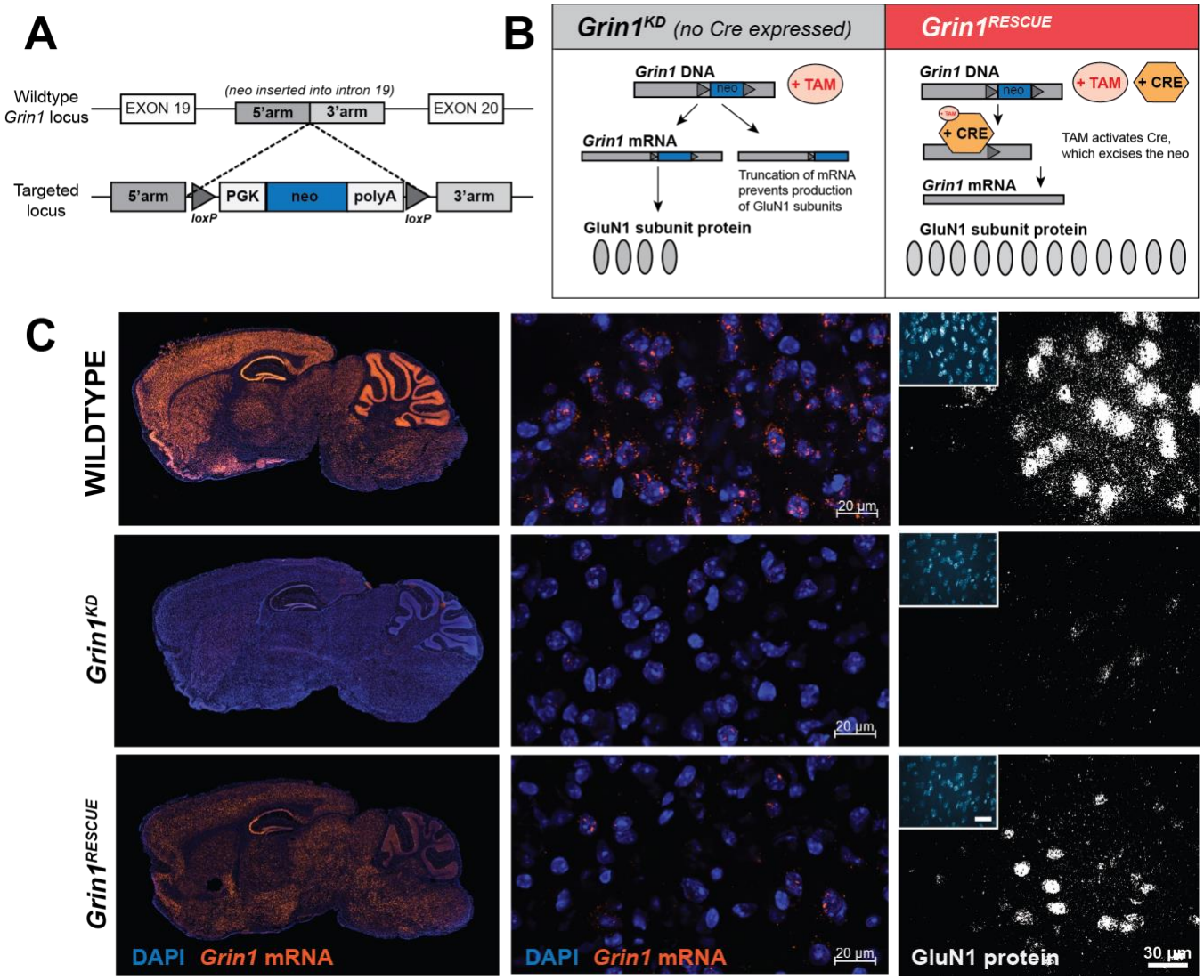

Figure 1. Generation and molecular characterization of the *Grin1* inducible-rescue mouse line. (A) Targeting construct schematic and recombination events at the *Grin1* locus in the generation of the *Grin1*$^{flneo/flneo}$ mouse model (top panel). PGK, PGK promotor; neo, neomycin selection cassette; polyA, polyadenylation sequence. **(B)** Schematic of expected molecular events at the *Grin1* locus. **(C)** RNAscope visualization of *Grin1* mRNA in mouse sagittal sections (20µm) via fluorescent in situ hybridization using *Grin1* probes *(left: whole brain; middle: 20x micrograph of prefrontal cortex)*. At right, sagittal sections (20µm) of prefrontal cortex visualizing GluN1 protein expression via fluorescent immunohistochemistry with a rabbit anti-GluN1 antibody (in-house, 1:200; secondary anti-rabbit Alexa 568) in WT, *Grin1*^{KD}, and *Grin1*^{RESCUE} mice.

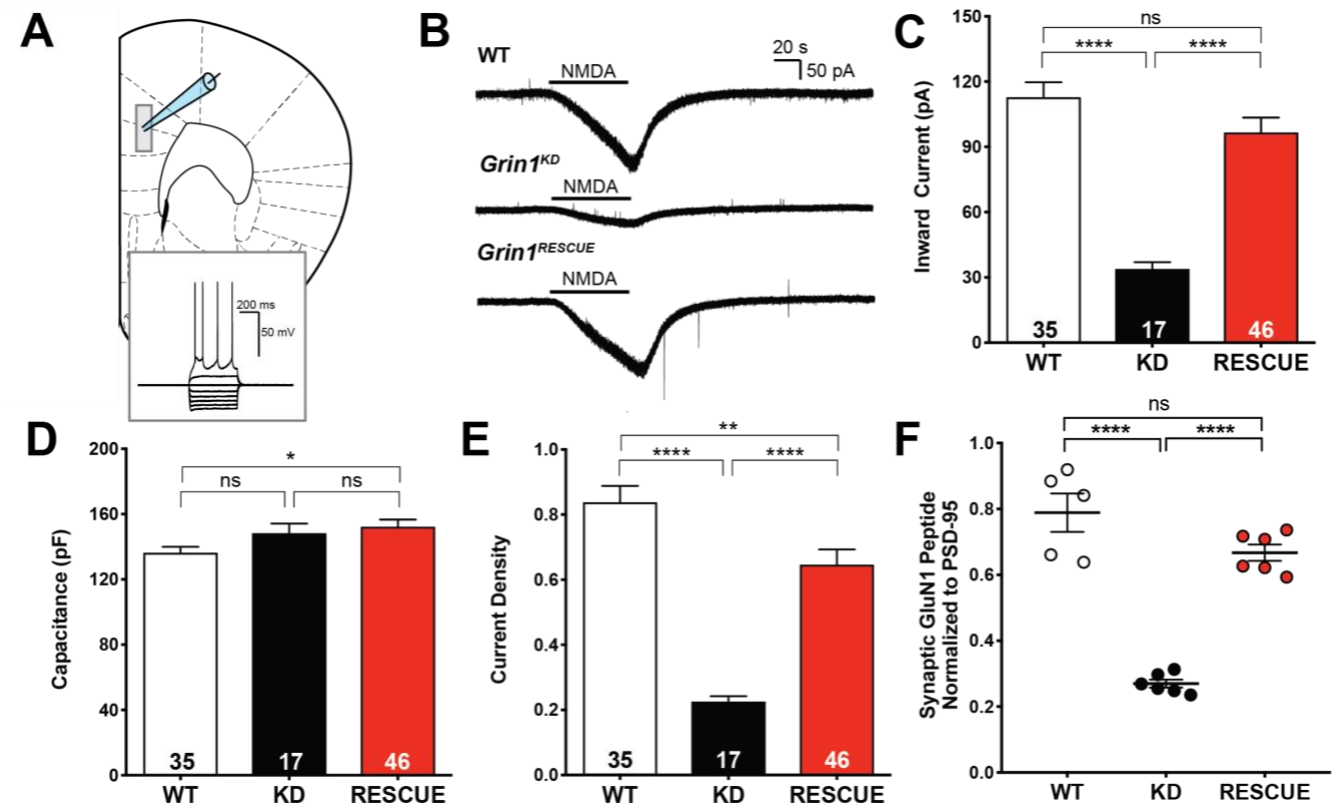

Figure 2. NMDAR currents and synaptic GluN1 peptide levels are restored in the PFC. (A) Schematic of mPFC with whole cell patch clamp recording from layer 5[36]. Inset: electrophysiological signature of *Grin1*^{RESCUE} layer 5 pyramidal neuron. **(B)** Representative traces in voltage-clamp (-75 mV) showing prefrontal response to NMDA across the three genotypes (number of layer 5 pyramidal neurons shown, 5-6 mice per genotype). **(C)** Quantification of peak amplitude of prefrontal NMDAR-elicited currents. Data shown as mean ± SEM, ****p<0.0001, ns=not significant, one-way ANOVA, effect of genotype, $F_{2,95}$ =22, p<0.0001, Bonferroni posthoc. **(D)** Capacitance of prefrontal layer 5 pyramidal neurons. Data shown as mean ± SEM, *p<0.05, ns =not significant, one-way ANOVA, Bonferroni posthoc. **(E)** Current density of prefrontal NMDA-elicited currents. Data shown as mean ± SEM, **p<0.01, ****p<0.0001, one-way ANOVA, effect of genotype, $F_{2,95}$ =3.6, p=0.03, Bonferroni posthoc. **(F)** Synaptic GluN1 peptide (IVNIGAVLSTR) levels in the PFC. Data shown as mean ± SEM, ****p<0.0001, ns=not significant, one-way ANOVA, effect of genotype, PFC: $F_{2,14}$ =64.76, p<0.0001, Bonferroni posthoc.

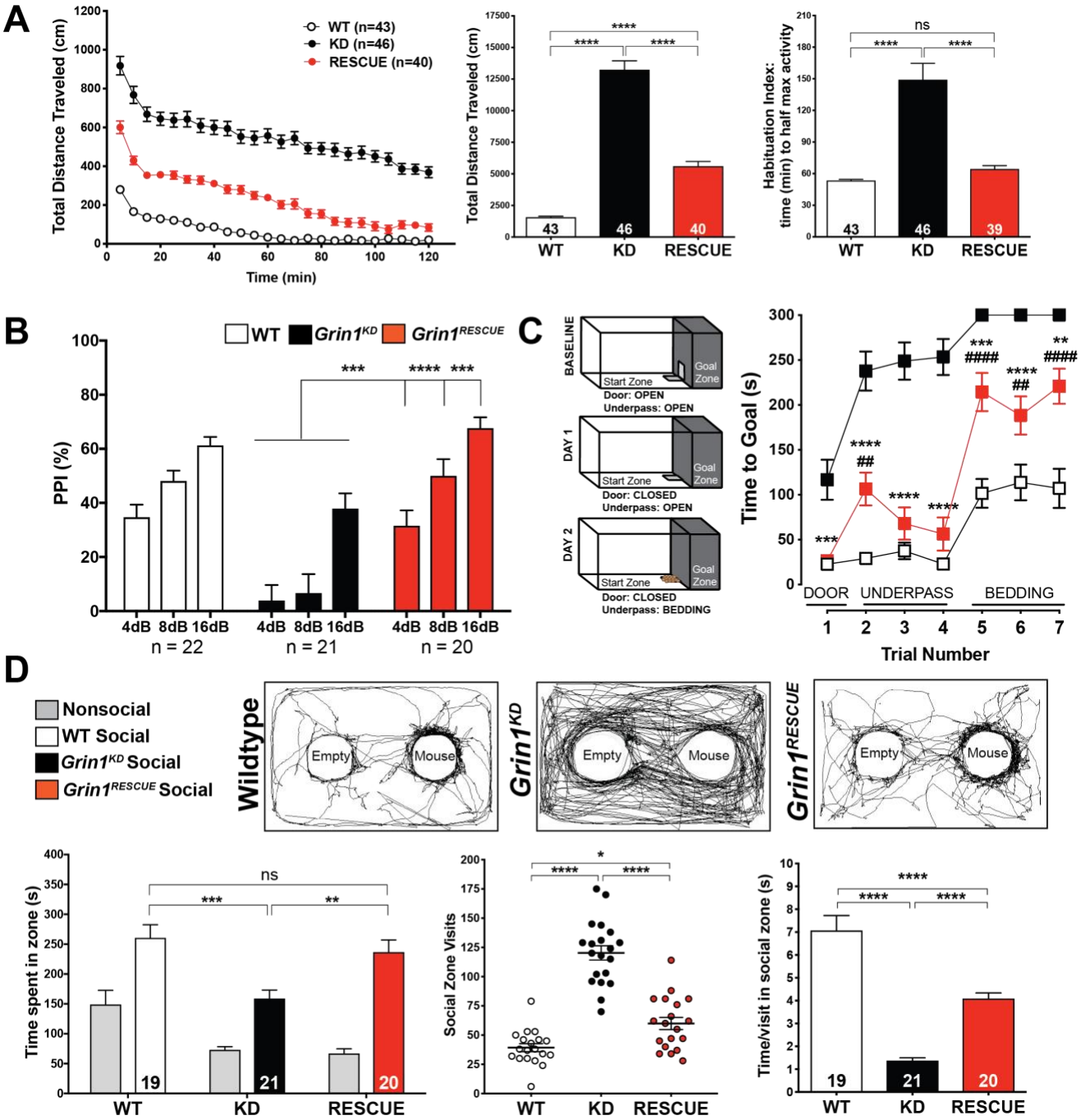

Figure 3. Cognitive symptoms show rescue following intervention. (A) Time-course and total distance traveled (cm) in open field (OF) test in WT, *Grin1*^{KD}, and *Grin1*^{RESCUE} mice. Data shown as mean ± SEM, ****p<0.0001, two-way ANOVA (time-course), one-way ANOVA (total), effect of genotype, $F_{3,164}$=176.34, p<0.0001, Bonferroni posthoc. Habituation index (time to reach half maximal activity) in OF test in WT, *Grin1*^{KD}, and *Grin1*^{RESCUE} mice. Data shown as mean ± SEM, ****p<0.0001, one-way ANOVA, effect of genotype, $F_{3,167}$=14.13, p<0.0001, Bonferroni posthoc. **(B)** Percent inhibition of startle response (PPI) in WT, *Grin1*^{KD}, *Grin1*^{RESCUE} mice. Shown on graph, *Grin1*^{KD} vs. *Grin1*^{RESCUE}: ***p<0.001, ****<0.0001, data shown as mean ± SEM, one-way ANOVA, effect of genotype: $F_{3,75}$= (4dB)8.81, p<0.001, (8dB)14.59, p<0.001, (16db)9.57, p<0.001, Bonferroni posthoc. **(C)** Schematic of puzzle box test. Time to reach goal zone (seconds; max 300sec) measured in puzzle box paradigm in WT, *Grin1*^{KD}, *Grin1*^{RESCUE} mice. Shown on graph, #WT vs. *Grin1*^{RESCUE}: ##p<0.01,

####p<0.0001; *$Grin1^{KD}$ vs. $Grin1^{RESCUE}$: **p<0.01, ***p<0.001, ****p<0.0001. Data shown as mean ± SEM, two-way ANOVA, effect of genotype: $F_{3,82}$=53.63, p<0.001, Bonferroni posthoc. N-values: WT – 21, $Grin1^{KD}$ – 25, $Grin1^{RESCUE}$ - 21 **(D)** Representative traces of modified three-chamber sociability. Total time spent, number of visits, and time per visit in the social zone during 10min. test, measured in WT, $Grin1^{KD}$, and $Grin1^{RESCUE}$ mice. Data shown as mean ± SEM, *p<0.05, **p<0.01, ***p<0.001, ****p<0.0001, ns = not significant, one-way ANOVA, effect of genotype: (time) $F_{3,75}$=7.14, p<0.0001, (visits) $F_{3,78}$=2.31, p<0.0001, (time/visit) $F_{3,77}$=12.55, p<0.0001, Bonferroni posthoc.

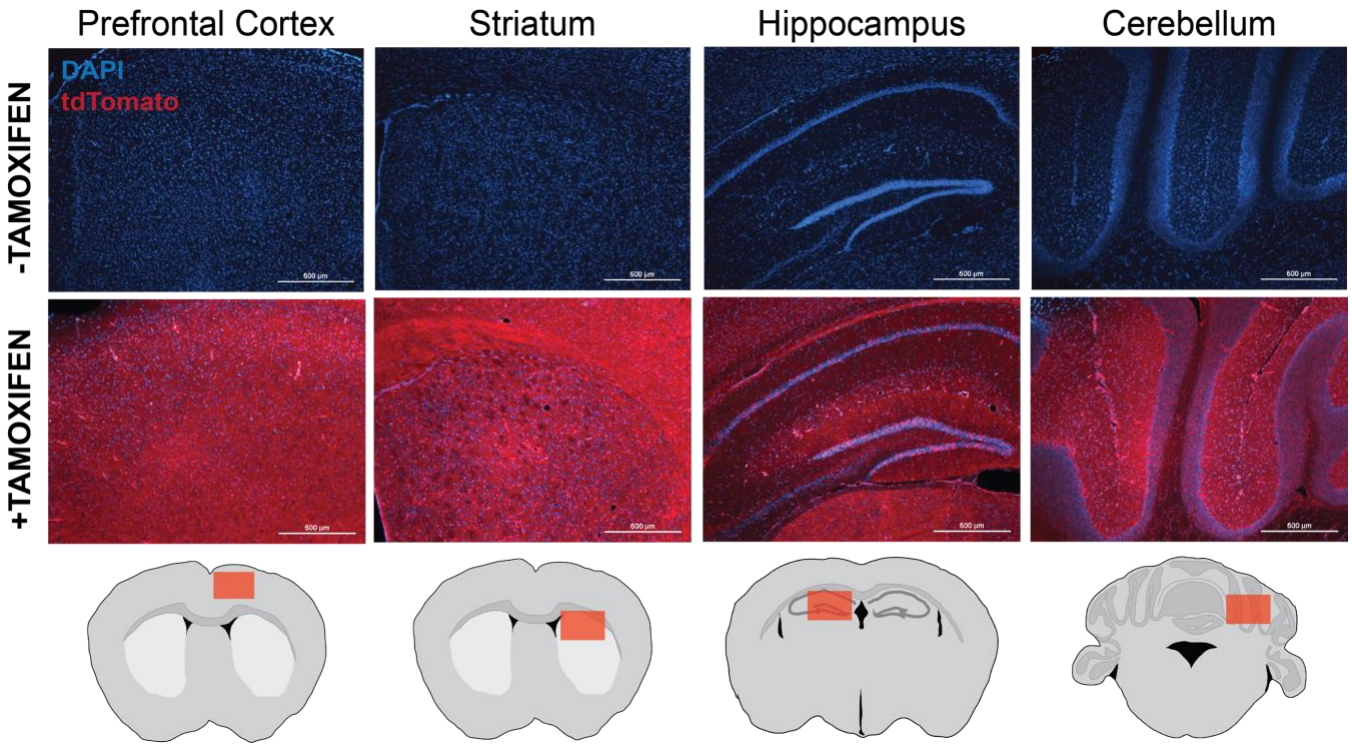

Extended Data Figure 1. Confirmation of tamoxifen-induced Cre recombinase expression. (A) Coronal sections (40µm) including mouse cortex, striatum, hippocampus and cerebellum visualizing tdTomato expression following Cre-mediated recombination in *ROSA26*$^{CreERT2/tdTomato}$ mice treated with TAM or vehicle.

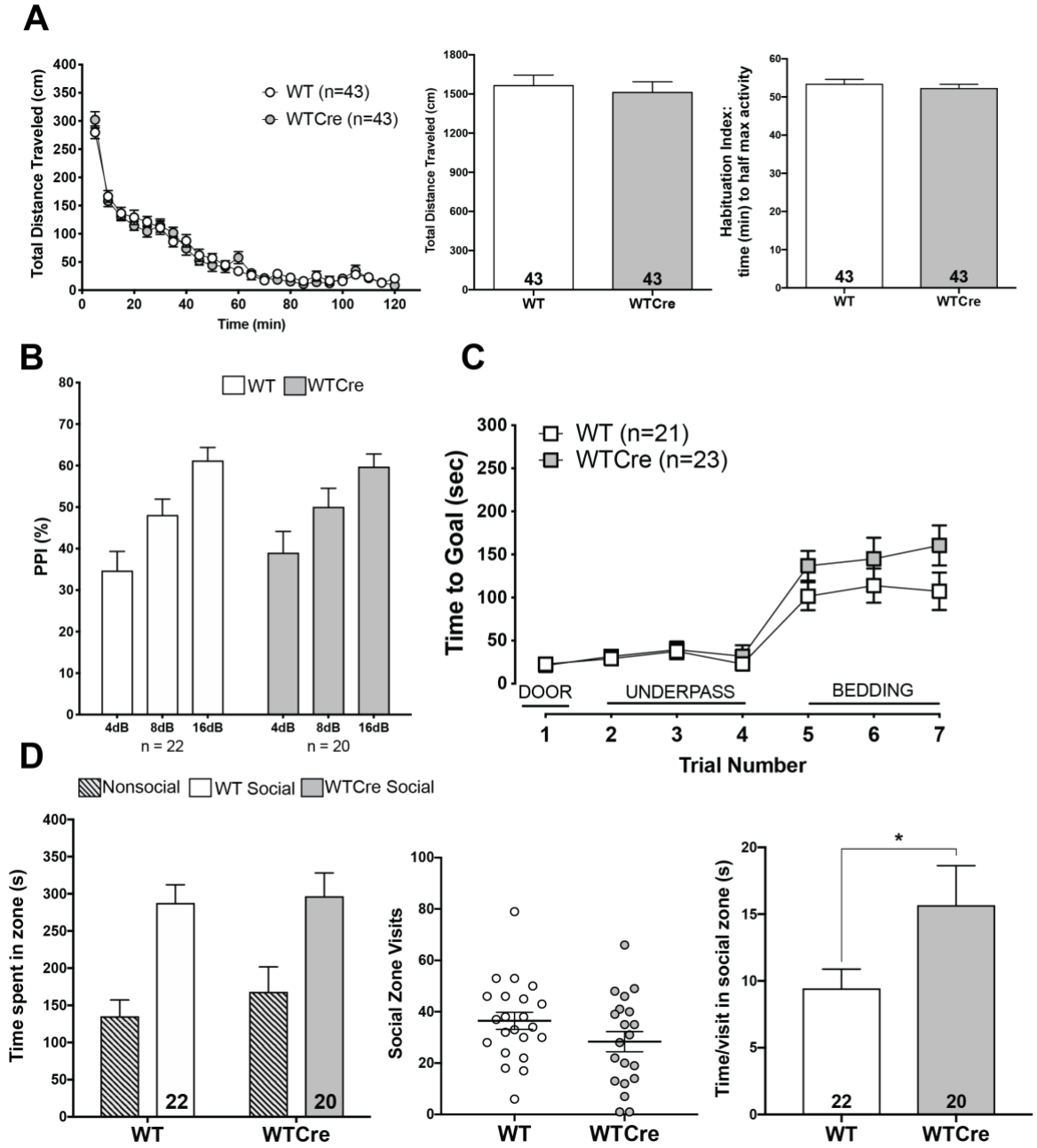

Extended Data Figure 2. Absence of behavioral differences between WT and WTCre mice. (A) Time-course, total distance traveled (cm), and time to reach half maximal activity in open field (OF) test over 120min. (5min. intervals) in WT and WTCre mice. Data shown as mean ± SEM, two-way ANOVA (all genotypes; time-course, multiple comparisons), one-way ANOVA (all genotypes; total, time to half max), Bonferroni posthoc. Total distance traveled: p>0.99, power=1.00; time to half max activity: p>0.99; power=0.99. **(B)** Percent inhibition of startle response (PPI) in WT and WTCre mice. Data shown as mean ± SEM, one-way ANOVA (each pre-pulse dB; all genotypes), multiple comparisons, Bonferroni posthoc. All decibels: p>0.99; power>0.99. **(C)** Time to reach goal zone (sec; max 300sec) measured in puzzle box paradigm in WT and WTCre mice. Data shown as mean ± SEM, two-way ANOVA (all genotypes), multiple comparisons, Bonferroni posthoc. All trials: p>0.99, power=1.00. **(D)** Total time spent in zone, number of visits to social zone, and time per visit in social zone in modified three-chamber sociability assay over 10min. in WT and WTCre mice. Data shown as mean ± SEM, one-way ANOVA, Bonferroni posthoc. Time spent in social zone: p>0.99, power=0.98; number of visits to social zone: p>0.99, power=1.00; time per visit in social zone: p=0.049, power=1.00.

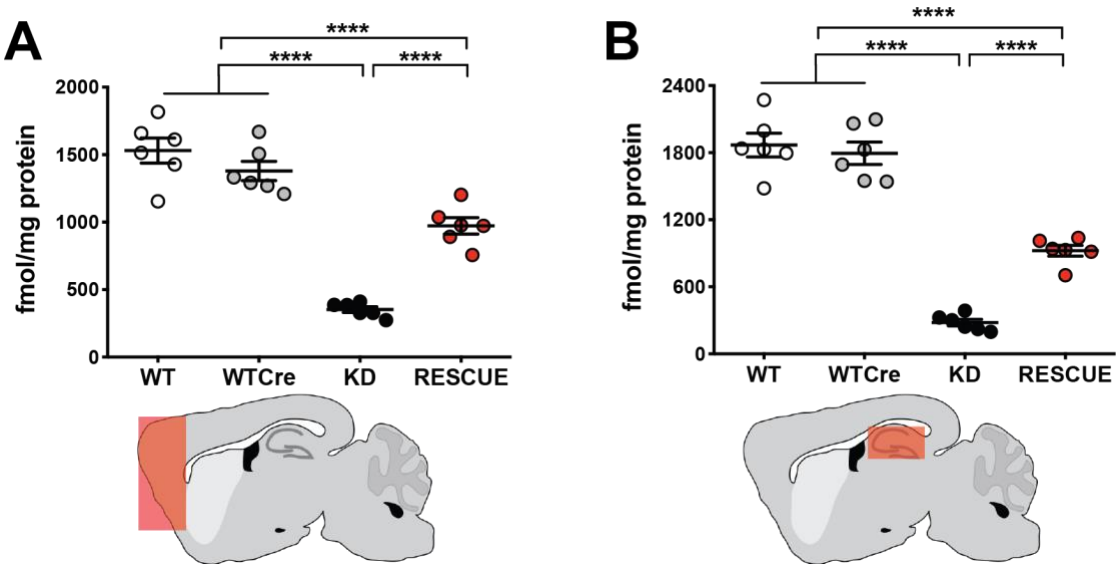

Extended Data Figure 3. NMDA receptor binding densities in mouse brain tissue. [^{3}H]MK-801 (fmol/mg) in brain tissue of WT, WTCre, *Grin1^{KD}* and *Grin1^{RESCUE}* mice in **(A)** cortex and **(B)**hippocampus. Binding assays were performed with the NMDAR antagonist MK-801 (hot and/or cold), mouse brain membranes (80µg) and binding buffer (total binding vs. non-specific binding), with a total assay volume of 150µl. Data shown as mean ± SEM, ****p<0.0001, one-way ANOVA, effect of genotype, $F_{3,20}$= (cortex) 1.305, p<0.0001, and (hippocampus) 2.045, p<0.0001, Bonferroni posthoc.

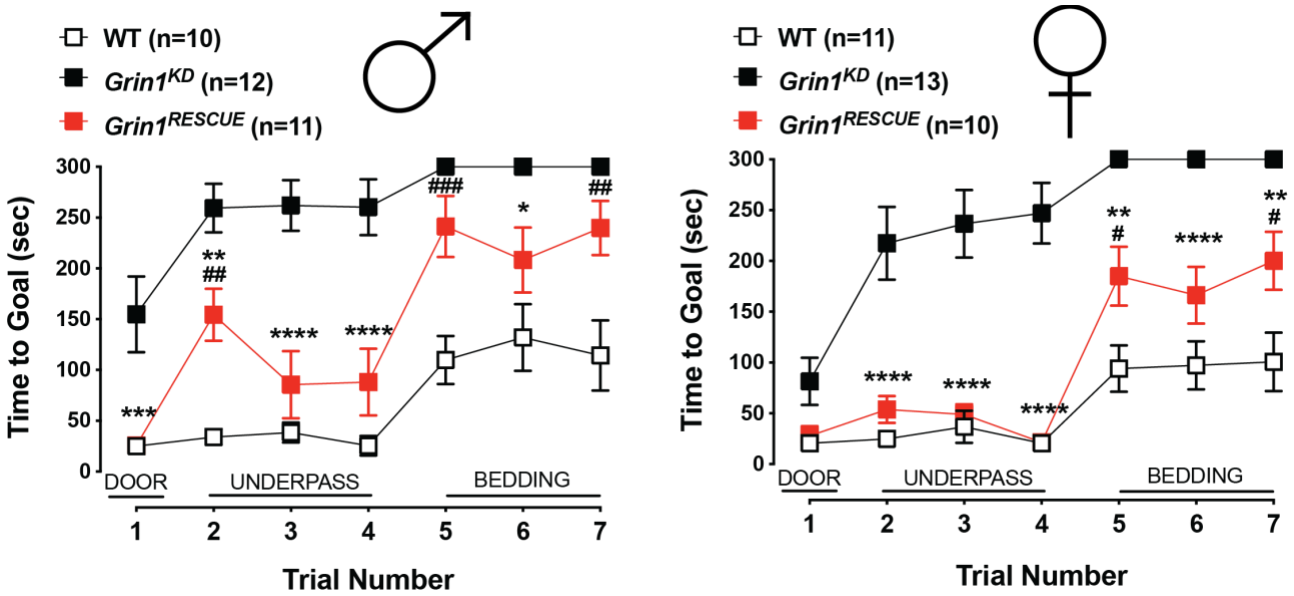

Extended Data Figure 4. *Grin1^{RESCUE}* females perform better in the puzzle box paradigm, when compared to *Grin1^{RESCUE}* males. Time to reach goal zone (sec; max 300sec) measured in puzzle box paradigm in WT, *Grin1^{KD}*, *Grin1^{RESCUE}* mice. Shown on graph, #WT vs. *Grin1^{RESCUE}*: ##p<0.01, ###p<0.001; **Grin1^{KD}* vs. *Grin1^{RESCUE}*: **p<0.01, ***p<0.001, ****p<0.0001. Data shown as mean ± SEM, two-way ANOVA, interaction of sex and genotype: $F_{3,82}$=2.941, p=0.038, Bonferroni posthoc.

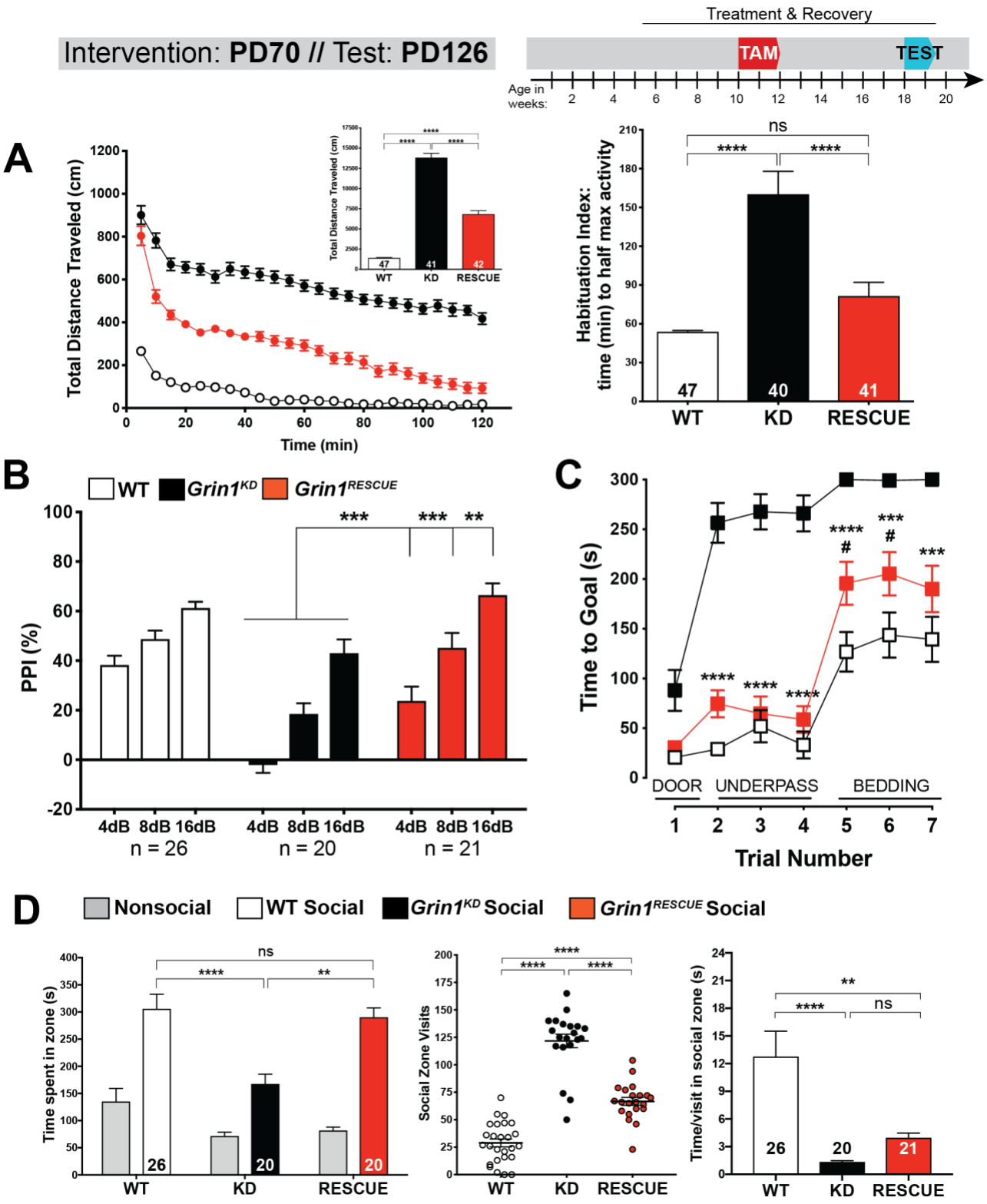

Extended Data Figure 5. Replicable and robust cognitive improvements following adult intervention with longer recovery time. (A) Time-course and total distance traveled (inset) in open field (OF) test in WT, *Grin1*^{KD}, and *Grin1*^{RESCUE} mice. Data shown as mean ± SEM, ****p<0.0001, two-way ANOVA (time-course), one-way ANOVA (total), effect of genotype, $F_{3,168}$=339.43, p<0.0001, Bonferroni posthoc. Habituation index (time to reach

half maximal activity) in OF test in WT, *Grin1*^{KD}, and *Grin1*^{RESCUE} mice. Data shown as mean ± SEM, ****p<0.0001, one-way ANOVA, effect of genotype, $F_{3,170}$=26.82, p<0.0001, Bonferroni posthoc. **(B)** Percent inhibition of startle response (PPI) in WT, *Grin1*^{KD}, *Grin1*^{RESCUE} mice. Shown on graph, *Grin1*^{KD} vs*. Grin1*^{RESCUE}: **p<0.01, ***p<0.001, data shown as mean ± SEM, one-way ANOVA, effect of genotype: $F_{3,80}$= (4dB)20.03, p<0.001, (8dB)11.33, p<0.001, (16db)6.03, p<0.001, Bonferroni posthoc. **(C)** Time to reach goal zone (seconds; max 300sec) measured in puzzle box paradigm in WT, *Grin1*^{KD}, *Grin1*^{RESCUE} mice. Shown on graph, #WT vs. *Grin1*^{RESCUE}: #p<0.05; **Grin1*^{KD} vs. *Grin1*^{RESCUE}: ***p<0.001, ****p<0.0001. Data shown as mean ± SEM, two-way ANOVA, effect of genotype: $F_{3,81}$=56.48, p<0.001, Bonferroni posthoc. N-values: WT – 26, *Grin1*^{KD} – 20, *Grin1*^{RESCUE} - 21 **(D)** Total time spent, number of visits, and time per visit in the social zone during 10min. test, measured in WT, *Grin1*^{KD}, and *Grin1*^{RESCUE} mice. Data shown as mean ± SEM, **p<0.01, ****p<0.0001, ns = not significant, one-way ANOVA, effect of genotype: (time) $F_{3,83}$=8.74, p<0.0001, (visits) $F_{3,83}$=96.87, p<0.0001, (time/visit) $F_{2,63}$=11.12, p<0.0001, Bonferroni posthoc.

Extended Data Table 1. **Intrinsic membrane properties of layer 5 pyramidal neurons in medial prefrontal cortex.**

	Prefrontal Cortex Layer 5 Pyramidal Neurons			
Membrane Properties	**WT**	***Grin1^{KD}***	***Grin1^{RESCUE}***	*P*
RMP (mV)	-76 ± 1	-76 ± 1	-77 ± 1	0.50
Capacitance (pF)	136 ± 4	148 ± 6	152 ± 4*	**0.03**
Input Resistance (MΩ)	101 ± 6	100 ± 12	92 ± 5	0.50
Spike Amplitude	89 ± 1	93 ± 1	88 ± 1	0.06

Properties were assessed rapidly after obtaining whole cell configuration. The data is expressed as mean ± SEM. Multiple comparisons one-way ANOVA with Bonferroni's post-hoc (*$p \leq 0.05$ compared to WT).

Extended Data Table 2. **NMDA receptor binding densities of [^{3}H]MK-801 (fmol/mg) in brain tissue of WT, *Grin1^{KD}* and *Grin1^{RESCUE}* mice.**

							Two-Way ANOVA					
	Wildtype		***Grin1^{KD}***		***Grin1^{RESCUE}***		Genotype		Intervention Time		Genotype*Intervention	
Intervention	**PD70**	**PD70+8**	**PD70**	**PD70+8**	**PD70**	**PD70+8**	*F*(3,46)	*P*	*F*(1,46)	*P*	*F*(3,46)	*P*
Cortex	1531.0	1679.0	352.2	385.2	972.8	956.1	111.967	**<0.001**	1.546	0.221	0.456	0.715
	± 92.6	± 137.2	± 20.9 23% WT	± 34.0 23% WT	± 60.6 63% WT	± 75.4 57% WT						
Hippocampus	1868.0	2051.0	279.2	254.9	922.7	994.0	60.391	**<0.001**	0.276	0.602	2.906	**0.046**
	± 105.9	± 200.0	± 28.9 15% WT	± 29.8 12% WT	± 48.2 49% WT	± 77.5 48% WT						

Data expressed as mean ± SEM in fmol/mg of protein. N=5-6/group, combined and equally balanced for sex. Multiple comparisons two-way ANOVA with Bonferroni's post-hoc.